eNeuro

Research Article: Methods/New Tools | Novel Tools and Methods

Realistic numerical and analytical modeling of light scattering in brain tissue for optogenetic applications

Modeling of light scattering in brain tissue

Guy Yona[a], Nizan Meitav[b], Itamar Kahn[c] and Shy Shoham[b]

[1]*Technion – Israel Institute of Technology, Autonomous Systems Program (TASP), Haifa, Israel*
[2]*Technion – Israel Institute of Technology, Faculty of Biomedical Engineering, Haifa, Israel*
[3]*Technion – Israel Institute of Technology, Faculty of Medicine, Haifa, Israel*

DOI: 10.1523/ENEURO.0059-15.2015

Received: 31 May 2015

Revised: 28 October 2015

Accepted: 30 October 2015

Published: 4 January 2016

Author Contributions: GY, IK and SS Designed Research, GY and NM Performed Research, GY and SS Analyzed Data and Wrote the Paper

Funding: Israel Ministry of Science, Technology and Space; ISF: 225/11. FP7-IRG: PCIG9-GA-2011-294001. Gutwirth Family fund;

Conflict of Interest: Authors report no conflict of interest.

Correspondence: Guy Yona, Technion – Israel Institute of Technology, Faculty of Medicine, Department of Neuroscience, 1 Efron st. POB 9649, Haifa 31096, Israel; Tel: +972 4-829-5463; E-mail: yona@tx.technion.ac.il and Shy Shoham, Technion – Israel Institute of Technology, Department of Biomedical Engineering, Technion City, Haifa 32000, Israel; Tel: +972 4-829-4125; E-mail: sshoham@bm.technion.ac.il

Cite as: eNeuro 2015; 10.1523/ENEURO.0059-15.2015

eNeuro

http://eneuro.msubmit.net

eN-MNT-0059-15R1

Realistic numerical and analytical modeling of light scattering in brain tissue for optogenetic applications

Manuscript Title Page

Manuscript Title:

Realistic numerical and analytical modeling of light scattering in brain tissue for optogenetic applications

Abbreviated Title: Modeling of light scattering in brain tissue

List all Author Names and Affiliations:

Guy Yona[a], Nizan Meitav[b], Itamar Kahn[c] and Shy Shoham[b]
[a]Technion – Israel Institute of Technology, Autonomous Systems Program (TASP), Haifa, Israel
[b]Technion – Israel Institute of Technology, Faculty of Biomedical Engineering, Haifa, Israel
[c]Technion – Israel Institute of Technology, Faculty of Medicine, Haifa, Israel

Author Contributions:

GY, IK and SS Designed Research, GY and NM Performed Research, GY and SS Analyzed Data and Wrote the Paper

Correspondence:

Guy Yona, Technion – Israel Institute of Technology, Faculty of Medicine, Department of Neuroscience, 1 Efron st. POB 9649 , Haifa 31096, Israel; Tel: +972 4-829-5463; E-mail: yona@tx.technion.ac.il

Shy Shoham, Technion – Israel Institute of Technology, Department of Biomedical Engineering, Technion City, Haifa 32000, Israel; Tel: +972 4-829-4125; E-mail: sshoham@bm.technion.ac.il

Number of Figures: 5

Number of Tables: 2

Number of Multimedia: 0

Number of words for Abstract: 164

Number of words for Significance Statement: 120

Number of words for Introduction: 709

Number of words for Discussion: 1075

Acknowledgements: The authors thank Prof. Ofer Yizhar for helpful discussions, Dr. Inbar Brosh for her technical assistance in producing the brain slices for the experiment, Shir Paluch for assistance with the BSF implementation and Eliran Guzi and Dalia Rifold for writing the simulation GUI.

Conflict of Interest: Authors report no conflict of interest

Funding sources: This work was supported by a grant from the Israel Ministry of Science, Technology and Space, ISF 225/11 (IK) and FP7-IRG PCIG9-GA-2011-294001 (IK). GY is supported in part by the Gutwirth Family fund.

Realistic numerical and analytical modeling of light scattering in brain tissue for optogenetic applications

Abstract

Optogenetics has in recent years become a central tool in neuroscience research. Estimating the transmission of visible light through brain tissue is of crucial importance for controlling the activation levels of neurons in different depths, designing the optical systems and avoiding lesions from excessive power density. The Kubelka-Munk model and Monte Carlo simulations have previously been used to model light propagation through rodents' brain tissue, however, these prior attempts suffer from fundamental shortcomings. Here, we introduce and study two modified approaches for modeling the distributions of light emanating from a multimode fiber and scattering through tissue, using both realistic numerical Monte Carlo simulations and an analytical approach based on the Beam Spread Function approach. We demonstrate a good agreement of the new methods' predictions both with recently published data, and with new measurements in mouse brain cortical slices, where our results yield a new cortical scattering length estimate of ~47 μm at λ = 473 nm, significantly shorter than ordinarily assumed in optogenetic applications.

Significance statement

For optogenetic stimulation to become highly controlled, reproducible and safe, a thorough understanding of the deep-tissue scattered light distributions that mediate the excitation is required. However, effective computation tools validated by actual measurements in brain tissue are currently still lacking. In this paper, we introduce, study and validate new numerical and analytical approaches for modeling the distributions of light propagating through brain tissue.

We show that both methods lead to consistent results and use the much faster analytical method to iteratively extract the optical parameters from new measurements, suggesting that light penetration into cortical tissue is significantly less than usually assumed. The new level of faithfulness could assist in designing experimental setups and optical interfaces, and help interpret optogenetics experiments.

Introduction

Optogenetic neuromodulation is playing an increasingly central role in neuroscience research and emerging applications (Deisseroth, 2011), with major efforts being directed towards the discovery and development of advanced optogenetic probes (Yizhar et al., 2011; Zhang et al., 2011) and related miniature devices (Deisseroth and Schnitzer, 2013). However, relatively little attention has been given to elucidating and characterizing the passage of light in brain tissue at the relevant visible wavelengths and illumination geometries: since light-tissue interactions at these wavelengths is strongly scattering-dominated, light transfer is heavily affected by multiple scattering events resulting in complex light distributions where the photons deviate considerably from their original directions. Estimating the resulting light distribution is of crucial importance for multiple aspects of optogenetic research including the control and analysis of neuronal excitation levels, comparison of the relative merits for different applications of probes with different excitation spectra, the design of effective optical systems for delivering sufficient light power density to target regions (Pashaie et al., 2014), and for avoiding lesions and light toxicity (Frigault et al., 2009) that may result from excessive light absorption.

Despite this central importance in interpreting and designing optogenetics experiments, methodical treatment of tissue light transport in this context has been sparse. To date, the central

84 approaches used for studying relevant scattered light distributions in rodent brains were based on
85 a Kubelka-Munk (KM) model fit to empirical results (Aravanis et al., 2007; Yizhar et al., 2011;
86 Adamantidis et al., 2007; Foutz et al., 2012), and on Monte Carlo (MC) simulations of light
87 transport (Bernstein et al., 2008; Chow et al., 2010; Kahn et al., 2011). Unfortunately, the
88 generality and applicability of each of these approaches suffers from major limitations. The KM
89 model (Kubelka, 1948) is a one dimensional model describing the propagation of light through a
90 diffuse scattering medium (with *no* absorption), based on two coupled differential equations that
91 describe the change in the intensity at each point in the slab based on the change of two fluxes:
92 the transmitted light flux and the backscattered flux. However, the KM model is based on
93 fundamental assumptions that are inconsistent with light scattering in tissue geometries and
94 length scales relevant to optogenetics**:** (1) it assumes isotropic scattering, which becomes true
95 only at the diffusive regime – depths of multiple millimeters, whereas at the distance scales and
96 wavelengths relevant to optogenetics, scattering is highly anisotropic; (2) it assumes isotropic
97 illumination (i.e. illumination from an infinite uniform plane), thus neglecting the finite
98 geometry and size of the illumination, which is typically of comparable size to the tissue of
99 interest. The various limitations of the KM model as suitable for capturing light scattering, are
100 extensively discussed by Neumann and Edstörm (2010). Likewise, the published MC
101 calculations (Bernstein et al., 2008; Chow et al., 2010; Kahn et al., 2011) were based on (very
102 different, see table 1) scattering parameters for *human* brains (Yaroslavsky et al., 2002), and are
103 unvalidated by empirical data (see discussion). More recently, more extensive sets of
104 measurements for estimating the optical parameters using different experimental strategies were
105 performed in several sub-cortical adult mouse brain areas (Al-Juboori et al., 2013) and in adult
106 rat brains (Azimipour et al., 2014). While important, broad empirical measurement datasets do

not provide the type of generality required for tackling a diversity of practical cases and designs, and leaves open the need for a complementary quantitative, practical and empirically validated modeling framework for optogenetic light propagation.

In this work, we apply two independent methods for *detailed* modeling of the transmission of light launched from a monochromatic optical fiber light source across various thicknesses of brain tissue: the MC method (Fang, 2010) and the Beam Spread Function (BSF) method (McLean et al., 1998), which is applied in this context for the first time. MC simulation uses repeated *numerical* random sampling while BSF is based on convolutions of an *analytical* beam propagation Green's function (an impulse response, which is used via the superposition principle to obtain a solution to more complex initial or boundary conditions). Despite the very different methodologies behind these two methods, we show that their results are both mutually consistent and in agreement with both published and new empirical brain-scattering results. Finally, we discuss the new approaches' relative merits and limitations, as well as directions for future study.

Methods

2.1 General considerations

In our models and in previous experiments (Yizhar et al., 2011; Aravanis et al., 2007), an optical fiber was located adjacent and perpendicular to an ex-vivo slice of mouse brain tissue. The fiber was emitting light in wavelength λ = 473 nm, its core radius was 100 μm and numerical aperture (NA) of 0.37. These parameters were also used by Aravanis et al. (2007). We assume that the spatial and angular intensity distributions of the emitted light at the fiber surface are uniform and constant. This assumption holds since the electric field distribution at the fiber tip is composed of

superposition of all the linearly polarized modes (amplitude distributions that remain unchanged during propagation in a fiber) supported by the fiber, which are very numerous. The number of modes (M) is typically estimated from the fiber's normalized frequency $V = 2\pi\left(\frac{r_{core}}{\lambda}\right)NA = 491.5$; (Okamoto, 2006), which indeed implies a very large number of modes $M \approx \frac{4}{\pi^2}V^2 \approx 10^5$. Another important parameter is the beam divergence at the fiber tip, since it determines the angular distribution of the light emanating from each point at the fiber tip. If we assume that the fiber is touching the tissue (i.e. no other interface between them), the half-angle of divergence θ_{div} is

$$\theta_{div} = \sin^{-1}\left(\frac{NA}{n_{tissue}}\right) = 15.8°,$$

where $n_{tissue} = 1.36$ is the refractive index of the brain tissue (Vo-Dinh, 2003). We assume a homogenous and isotropic (i.e. there is no preferable direction in the tissue) scattering tissue, characterized by a scattering coefficient μ_s (cm^{-1}), a weak absorption coefficient μ_a (cm^{-1}, $\mu_a << \mu_s$), and a high anisotropy coefficient g (dimensionless) which represents a tendency for strongly forward scattering at each scattering event. Using the two methods described below, we calculate local intensity (the radiant power passing through a unit surface) in different points across the tissue.

2.2 Monte Carlo simulation

The MC simulation is based on the Mesh-based Monte Carlo (MMC) code developed by Fang (2010), version 0.9.5. Since the MMC software is based on an infinitely narrow beam (pencil beam) light source, we adapted it to a more complex light source using a three-step process:

a. The 3D pencil beam response was produced by simulations performed at a logarithmic lateral resolution spanning from 1.2 µm near the central beam to 47 µm at the edge of the

simulated volume, and an axial resolution of 5 µm, with 10^8 simulated photons. The response was then resampled by a uniform isotropic grid of 5 µm.

b. The 3D pencil beam response was rotated in 64 intervals over the inclination angle θ_{div} along the rotation axis, which is the entrance point of the pencil beam into the tissue. Sequentially, the result was rotated over a full circle in 64 intervals along the azimuthal direction. The results of all the rotations were summed up to form the angular light pattern that was emitted from each point of the fiber tip (Figure 2a). In effect, the rotations can be formulated in terms of angular convolution with unit vectors that span the inclination angles $[0, \theta_{div}]$ and the azimuth angles $[0,2\pi]$.

c. To take into account the fiber tip area, the result of the previous stage was convolved with a sampled disk of the same diameter as the fiber (Figure 2a).

2.3 Beam spread function simulation

The (BSF) method (McLean et al., 1998) is a uniquely powerful solution for approximating light distributions in highly forward scattering media where the higher-order effects of photons coming via multiple paths of various lengths, thus resulting in *time dispersion* of the light intensity, is also incorporated. The method applies an analytical approximation for unidirectional pulsed source propagation in a turbid medium, which serves as a Green's function that can be used to solve more general problems (i.e. via angular and spatial convolution): the BSF $k(z, \boldsymbol{\rho}, \tau)$ is the intensity distribution of light from a pulsed source normalized to the pulse's energy, after propagating a distance z in the medium, where $\boldsymbol{\rho}$ is the radial position vector, and $\tau = t - z/c$ is the multipath time (c is the speed of light in the medium, t is the time since the photons start propagating, $\tau = 0$ for unscattered photons). McLean *et al.* (1998) present a useful decomposition of the scattered photons BSF into a product of a normalized temporal dispersion distribution

function $G(z,\tau)$ and a normalized spatial-angular distribution function $h(z,\boldsymbol{\rho},\tau)$ (see upper part of Figure 1),

$$k_{sc}(z,\boldsymbol{\rho},\tau) = e^{-\mu_a(z+c\tau)}G(z,\tau)\cdot h(z,\boldsymbol{\rho},\tau) \quad (1)$$

where μ_a is the absorption coefficient. Following McLean *et al.* (1998), we use the time-dependent spatial distribution function (derived from the time-independent small-angle approximation):

$$h(z,\boldsymbol{\rho},\tau) = \frac{3}{4\pi\tau cz}\exp\left(-\frac{3}{4}\frac{\boldsymbol{\rho}^2}{\tau cz}\right), \quad (2)$$

and the Gamma probability density function is used as the temporal distribution function (equivalent to a normal distribution when the variable, τ, is positive definite):

$$G(z,\tau) = \frac{\mu}{\sigma^2\Gamma\left(\frac{\mu^2}{\sigma^2}\right)}\left(\frac{\mu\tau}{\sigma^2}\right)^{\frac{\mu^2}{\sigma^2}-1}\exp\left(-\frac{\mu\tau}{\sigma^2}\right), \quad (3)$$

where μ and σ are the first and second moments of τ, respectively, and are dependent only on the first and second moments of the cosine of the scattering angle θ (see McLean et al., 1998 for formulas), and $\Gamma(x)$ is the gamma function. The BSF of the scattered photons, $k_{sc}(z,\boldsymbol{\rho},\tau)$ was calculated for the tissue optical parameters (same as for the MC method) and integrated over time. The unscattered photons were added next to obtain the combined BSF (see lower part of Figure 1):

$$k(z,\boldsymbol{\rho},\tau) = \delta(\boldsymbol{\rho})\delta(\tau)e^{-(\mu_a+\mu_s)z} + (1-e^{-\mu_s z})\,k_{sc}(z,\boldsymbol{\rho},\tau). \quad (4)$$

Subsequently, angular and spatial convolutions were performed to obtain the propagation of light from the fiber's tip, as was done with the MC method (only steps 2 and 3 are required here, since the Green's function is calculated for the entire volume, see Figure 2).

The calculation of the BSF pencil beam is considerably faster than MC calculation with comparable accuracy (several seconds compared to hours). As a result, curve fitting can be more readily used to obtain the optical parameters of a sample. We implemented the accelerated gradient search method (Beck and Teboulle, 2009) to find the scattering coefficient and anisotropy factor of the published data manually extracted from Aravanis et al. (2007) and of our measurements (Figure 5 below).

2.4 Experimental setup

All procedures were conducted in accordance with the national ethics committee for animal experimentation and with the approval of the Committee on Animal Care at The Technion – Israel Institute of Technology. Mouse brain slices were illuminated from above with a blue laser (473 nm) emanating from a fiber of 200 µm in diameter with NA of 0.37 (Thorlabs BFL37-200, Newton, NJ). The light intensity was measured through a small aperture (about 50 µm in diameter) using a power meter (Newport 818-ST, Irvine, CA), when the fiber tip is adjacent to the slice surface, above the point of maximal intensity (Figure 2c). Oblique, semi-coronal brain slices were obtained from 2 female mice (5 months old, C57/BL6 strain) from the same litter. The slice thicknesses used were 150, 200, 300, 400, 500 and 600 µm. Four measurements per slice were taken in neocortical areas, with 2-3 slices of each thickness obtained per animal ($n =$ 16 to 20 for each slice thickness). Since we found greater scattering near the white-matter at the deep layers of the cortex, the measurements were performed at central locations. The slices and the fiber were submerged in artificial cerebro-spinal fluid (aCSF) throughout the measurements, and were oxygenated until shortly before the measurement. In addition, radial intensity profile was obtained for the 300 µm and 600 µm thick slices, by moving the fiber tip laterally in 50µm intervals to 1mm. The measured results were normalized to the measured light intensity without

the slice (at the same height above the aperture) divided by the theoretical predicted attenuation due to geometric beam spreading.

Results

We first examined the accuracy of BSF method by comparing it to MC simulation results using two sets of previously published brain tissue optical parameters: scattering coefficient μ_s =168.6 cm^{-1} from Al-Juboori et al. (2013) measured in the mouse's pedunculopontine nucleus using 453 nm blue light at the top, and μ_s =120 cm^{-1} from Yaroslavsky et al. (2002) measured in human brain gray-matter tissue using 480 nm blue light at the bottom. Figure 3a shows contour maps of the calculated light transmission using the MC method, and Figure 3b shows the same using the BSF method. The fiber diameter used for the models in this figure is 100 μm and the NA is 0.22 (as reported by Al-Juboori et al.). Due to lack of better data, we used the absorption coefficient and anisotropy factor of native human gray matter from Yaroslavsky et al. (2002), μ_a = 0.6 cm^{-1} and g = 0.88 in both cases. These results illustrate that the analytical BSF method generally follows the MC predictions quite closely for a parameter regime which is relevant for optogenetics.

Next, we compared the models' predictions to two published experimental accounts on transmission along the z-axis, that is, the fiber's central axis (Figure 3; Aravanis et al., 2007; Al-Juboori et al., 2013). First, we compared the models' results of Figure 3c to the published decay curves by Al-Juboori et al. (Figure 4b). As discussed above, the results of the MC and the BSF methods are in excellent agreement (root mean square [rms] transmission error of 0.52% over the range 0–1mm), and we find that both provide a very good fit to the experimental measurements (rms error of 0.97% over the range 0-0.3 mm). In contrast, the model-based simulations are in

poor agreement with the experimental measurements of Aravanis et al. (2007). The comparison used the experimental setup geometry of Aravanis et al. (2007), where the fiber tip remained in a fixed height while the tissue samples being replaced, and no aperture was used. It can be shown that the light attenuation curve obtained this way is equivalent to depicting the integrated light intensities over the entire layers. A version of the BSF model was adapted to implement this integration, and best-fit curves to the data from Aravanis et al. (2007) used this modification. The obtained optical parameters were: scattering coefficient 60.7 cm^{-1}, absorption coefficient 0.62 cm^{-1} and anisotropy factor g = 0.89.

Finally, we compared model-based predictions to the new set of measurements performed in adult mouse cortical slices (Figure 5). In order to estimate the tissue's scattering parameters, we searched for a BSF model that simultaneously provided the best-fit to both the axial and lateral profiles (obtained parameters: scattering coefficient 211 cm^{-1} and anisotropy factor g = 0.86). The results again demonstrate an excellent agreement between the respective simulation methods, and between them and the experimental curves. Overall, these results exhibit a strong attenuation of the light intensity along the z axis due to multiple scattering: the intensity is reduced to 50% at a depth less than 40 µm, and to just a few percent at depths exceeding 200 µm (mean free path is 47 µm). This finding highlights how the gray matter's high density leads to a large number of scattering events over a relatively very short distance.

Discussion

In this study we sought to develop and experimentally validate solutions for realistic modeling of optogenetic light delivery using an optical fiber embedded in brain tissue. MC simulations, a generally accepted numerical method for simulating light propagation in biological tissues (Zhu

and Liu, 2013), have already been extensively applied to this problem, however, generally using inappropriate tissue parameters (see Table 1) and without capturing the input light source's spatial and angular properties; these issues are particularly important in light of the general lack of experimental validation of simulation results. Additionally, we adapted and extended a powerful analytical method for estimating scattered light distributions, the BSF, and carefully compared it to the MC results and to experimental measurements. Importantly, the results of the analytical solutions were found to be highly consistent with the MC simulation results, with the published attenuation profile measurements by Al-Juboori et al. (2013) in mouse sub-cortical regions (Figure 4b), and with a new set of cortical attenuation measurements (Figure 5). The model-based iso-intensity contours in cortical slices (Figure 5d) are also in rough agreement with the measured results found in Yizhar et al. (2011; their Figure 3E), which is itself in stark disagreement with the attenuation graph of Aravanis et al. (2007; reproduced in Figure 3B in Yizhar et al. 2011). Our method for measuring and estimating the parameters uses a geometry and fits to localized measurements that are directly relevant to optogenetics and does not rely on the multiple assumptions behind diffuse reflectance estimates (Azimipour et al. 2014).

The very good inter-model agreement found is probably as good as one can obtain, given that there are several reasons to expect small discrepancies between the two methods. First, the BSF formulation uses several approximations and assumptions. For example, the temporal probability density is modeled as a Gamma distribution, although more recent work (Funk and Pfeilsticker, 1999; Theer and Denk, 2006) suggests the lognormal distribution may be a more accurate model. Moreover, the methods have some inherent numerical errors, especially as a result of integration, interpolations, and the limited volume (spatial, temporal and directional) allocated for the Green

function. Likewise, differences from the empirical measurements can be attributed to tissue inhomogeneity, approximations in the experimental setup (e.g., neglecting the polystyrene and air layers between the slice and the detector, errors in slice thickness, etc.), and errors in the estimated optical parameters used. Finally, while the methods were applied here to a uniform light source, it can be easily accommodated to other beam profiles (e.g. Gaussian beam, multiple fibers, etc.). It is, however, important to note that like almost all current methods that describe the propagation of light in a turbid media, both methods do not take the wave properties of the light into account; thus, when using a coherent source, the interference of photons with different phases (due to different optical path lengths) will form a speckle pattern that can also reduce the total illumination level at each position.

Using the new BSF method, the scattering coefficient and anisotropy factor were estimated in measurements performed in mouse cortical slices. This estimation procedure was based on simultaneously optimizing the MSE fit to both the axial and two lateral curves (Figure 5) using only two scattering parameters (or 'degrees of freedom'). This iterative fit procedure was facilitated by the tremendous speed gain of the BSF method relative the MC numerical simulations (~10 seconds/BSF computation vs. ~10 hours/MC to achieve a comparable accuracy on a modern desktop PC).

Table 1 compares our results to estimates of these parameters based on the published data by Aravanis et al. (2007), as well as related parameter estimates obtained in the adult mouse pedunculopontine tegmental nucleus (Al-Juboori et al., 2013), in adult rat cortex (Figure 5; Azimipour et al., 2014) and in human gray matter (Yaroslavsky et al., 2002). This comparison

illustrates the much stronger scattering in mouse cortex seen in our results than indicated by Aravanis et al. (2007) and is generally more consistent with the stronger scattering observed by Al-Juboori et al. (2013) and Azimipour et al. (2014). Noting the considerable difference in the optical parameters between human and mouse brains, and between brain areas, we advise to refrain from using them interchangeably. Indeed, these findings explain the observations in Bernstein et al. (2008), who report a ratio of ~0.73 in the diameters of the 1% and 10% contours of light attenuation between their measurements in mouse brain slices and MC simulations, which were based on human brain optical parameters. Note, however, that these estimates should be used with caution if scattering is expected to change. For example, measurements should be

Source	**Brain sample**	**Wavelength (nm)**	**Scattering coef. (cm^{-1})**	**Anisotropy factor**
Own experiment	adult mouse cortex, (5 months old)	473	211	0.86
Aravanis	mouse cortex	473	60.7	0.885
Al-Juboori	mouse subcortical, (6-8 week old)	453	168.6	-
Azimipour	rat cortex	532	~170	~0.9
Yaroslavsky	human gray matter	480	120	0.88

Table 1: Brain tissue optical parameters

performed on tissue samples obtained from younger animals, as their scattering has been shown to be weaker (Oheim et al., 2001).

These results therefore put forward the BSF as a viable analytical approach towards a better understanding of light propagation and interactions in optogenetics and related fields, while use of the Kubelka-Munk model should be discouraged due to its theoretical inadequacy. As we have

shown, the BSF can be used both for calculating the light distribution in brain tissue, and for estimating the optical parameters from measured attenuation curves. Since the BSF is an analytical method, it is considerably faster than a MC simulation, enabling its implementation to curve fitting algorithms that obtain the optical parameters of the tissue and require multiple calculations of the attenuation curve with different parameters. A major limitation of light propagation models in brain tissue (including the ones portrayed here) is the assumption of homogeneity, whereas the cortical layers have different cytological properties, and necessarily also different optical parameters. These can be obtained in a similar manner, by performing the attenuation curve fitting *in parts* using the histological layers depths. A useful, immediate application of the BSF method for experiment design, is to determine the tissue volume illuminated to various levels by different optical fibers (Table 2). It is noted that exact calculation of the light intensity inside the tissue is a prerequisite for determining the excitation from optogenetic stimulation, but does not completely describe the excitation from optogenetic light. In order to estimate the excitation properly, one has to know the cell morphology, the distribution of the light-sensitive channels and the baseline excitability from sub-threshold oscillations. Moreover, *in vivo* optogenetic stimulation is also prone to absorption by blood (Azimipour et al., 2015), which is highly non-homogenous and remains untreated in our model.

Fiber properties		Volume illuminated ($10^{-3} \times mm^3$)			
NA	**Diameter (µm)**	**>50%**	**>20%**	**>5%**	**>1%**
0.1	25	0.02	0.04	0.09	0.20
0.22	50	0.06	0.14	0.34	0.79
0.22	105	0.29	0.68	1.48	3.28
0.22	200	1.07	2.56	5.53	13.7
0.22	365	3.62	8.71	19.5	61.7
0.37	200	1.05	2.52	5.52	14.3
0.39	200	1.05	2.51	5.50	14.4
0.39	300	2.39	5.75	12.7	38.1
0.39	400	4.30	10.4	23.3	79.4
0.48	400	4.76	10.3	23.1	79.0

Table 2: The illuminated tissue volumes for various commercial optical fibers. Threshold is in percent of maximal illumination.

A BSF solver is available at niel.net.technion.ac.il/software.

353 **References**

354 Adamantidis AR, Zhang F, Aravanis AM, Deisseroth K, de Lecea L (2007) Neural substrates of
355 awakening probed with optogenetic control of hypocretin neurons. Nature 450:420-424.

356 Al-Juboori S, Dondzillo A, Stubblefield EA, Felsen G, Lei TC, Klug A (2013) Light scattering
357 properties vary across different regions of the adult mouse brain. PLoS ONE 8:e67626.

358 Aravanis AM, Wang LP, Zhang F, Meltzer LA, Mogri MZ, Schneider MB, Deisseroth K (2007)
359 An optical neural interface: In vivo control of rodent motor cortex with integrated fiberoptic and
360 optogenetic technology. J Neural Eng (England) 4:S143-56.

361 Azimipour M, Atry F, Pashaie R (2015) Effect of blood vessels on light distribution in
362 optogenetic stimulation of cortex. Opt Lett 40:2173-2176.

363 Azimipour M, Baumgartner R, Liu Y, Jacques SL, Eliceiri K, Pashaie R (2014) Extraction of
364 optical properties and prediction of light distribution in rat brain tissue. - BIOMEDO 19:075001.

365 Beck A, Teboulle M (2009) A fast iterative shrinkage-thresholding algorithm for linear inverse
366 problems. SIAM J.Img.Sci. 2:183-202.

367 Bernstein JG, Han X, Henninger MA, Ko EY, Qian X, Franzesi GT, McConnell JP, Stern P,
368 Desimone R, Boyden ES (2008) Prosthetic systems for therapeutic optical activation and
369 silencing of genetically-targeted neurons. Proceedings - Society of Photo-Optical
370 Instrumentation Engineers 6854:68540H-68540H.

371 Chow BY, Han X, Dobry AS, Qian X, Chuong AS, Li M, Henninger MA, Belfort GM, Lin Y,
372 Monahan PE, Boyden ES (2010) High-performance genetically targetable optical neural
373 silencing by light-driven proton pumps. Nature 463:98-102.

374 Deisseroth K (2011) Optogenetics. Nature Methods 8:26-29.

375 Deisseroth K, Schnitzer M (2013) Engineering approaches to illuminating brain structure and
376 dynamics. Neuron 80:568-577.

377 Fang Q (2010) Mesh-based monte carlo method using fast ray-tracing in plucker coordinates.
378 Biomedical Optics Express 1:165-175.

379 Foutz TJ, Arlow RL, McIntyre CC (2012) Theoretical principles underlying optical stimulation
380 of a channelrhodopsin-2 positive pyramidal neuron. J Neurophysiol (Bethesda, MD) 107:3235-
381 3245.

382 Frigault MM, Lacoste J, Swift JL, Brown CM (2009) Live-cell microscopy - tips and tools. J
383 Cell Sci (England) 122:753-767.

384 Funk O, Pfeilsticker K (1999) Photon path length distributions for cloudy skies - oxygen A-band
385 measurements and model calculations. Ann Geophys 21:615-626.

386 Kahn I, Desai M, Knoblich U, Bernstein J, Henninger M, Graybiel AM, Boyden ES, Buckner
387 RL, Moore CI (2011) Characterization of the functional MRI response temporal linearity via
388 optical control of neocortical pyramidal neurons. J Neurosci (United States) 31:15086-15091.

389 Kubelka P (1948) New contributions to the optics of intensely light-scattering materials. part I. J
390 Opt Soc Am 38:448-448.

391 McLean JW, Freeman JD, Walker RE (1998) Beam spread function with time dispersion. Appl
392 Opt 37:4701-4711.

393 Neuman M, Edström P (2010) Anisotropic reflectance from turbid media. I. Theory, J. Opt. Soc.
394 Am. A 27(5):1032-9

395 Oheim M, Beaurepaire E, Chaigneau E, Mertz J, Charpak S (2001) Two-photon microscopy in
396 brain tissue: Parameters influencing the imaging depth. J Neurosci Methods 111:29-37.

397 Okamoto K (2006) Fundamentals of optical waveguides. Burlington, MA: Elsevier.

398 Pashaie R, Anikeeva P, Jin Hyung Lee, Prakash R, Yizhar O, Prigge M, Chander D, Richner TJ,
399 Williams J (2014) Optogenetic brain interfaces. Biomedical Engineering, IEEE Reviews In 7:3-
400 30.

401 Theer P, Denk W (2006) On the fundamental imaging-depth limit in two-photon microscopy. J
402 Opt Soc Am A 23:3139-3149.

403 Vo-Dinh T (2003) Biomedical photonics handbook. Boca Raton, FL: CRC Press.

404 Yaroslavsky AN, Schulze PC, Yaroslavsky IV, Schober R, Ulrich F, Schwarzmaier HJ (2002)
405 Optical properties of selected native and coagulated human brain tissues in vitro in the visible
406 and near infrared spectral range. Phys Med Biol (England) 47:2059-2073.

Yizhar O, Fenno LE, Davidson TJ, Mogri M, Deisseroth K (2011) Optogenetics in neural systems. Neuron (United States) 71:9-34.

Zhang F, Vierock J, Yizhar O, Fenno LE, Tsunoda S, Kianianmomeni A, Prigge M, Berndt A, Cushman J, Polle J, Magnuson J, Hegemann P, Deisseroth K (2011) The microbial opsin family of optogenetic tools. Cell 147:1446-1457.

Zhu C, Liu Q (2013) Review of monte carlo modeling of light transport in tissues. J Biomed Opt (United States) 18:50902.

Figure 1. Graphical depiction of the beam spread function (BSF) calculation process: the distribution of the scattered photons $k_{sc}(z,\rho,\tau)$ is a product of the spatial distribution $h(z,\rho,\tau)$ and the temporal dispersion distribution $G(z,\tau)$ (eq. 1). The time-dependent distribution is integrated over time to obtain the intensity values $k_{sc}(z,\rho)$,and added to the distribution of the unscattered photons $k_{usc}(z,\rho)$ for the total distribution $k(z,\rho)$ (eq. 4), called the BSF. Note that the equations also include absorption effects that were omitted from the figure for simplicity.

Figure 2. (a) Simulation procedure: the 1st stage is the calculation of a 3D pencil beam response, the 2nd stage is the angular convolution of the pencil beam response, and the 3rd stage is a spatial convolution with the fiber tip area; (b) Simulation outcomes of the various simulation steps. For better visualization all the figures are in log scale; (c) Illustration of the experimental setup cross-section.

Figure. 3. Comparisons of MC and BSF methods for two different tissue scattering parameter settings: μ_s =168.6 cm^{-1} (top, from Al-Juboori et al. 2013) and μ_s =120 cm^{-1} from (bottom, Yaroslavsky et al. 2002). (a) Contour maps of the light distribution in the tissue, created using the MC method; (b) Contours created using the BSF method. The iso-intensity lines are at 50%, 20%, 5%, and 1% of maximum. (c) Light transmission curves along the z-axis.

Figure. 4. Transmission of light along the z-axis, comparing published experimental results (red dotted curves) with BSF method (blue curves). (a) Best-fit curves to measured data from Aravanis et al. (2007). (b) Experimental data from Al-Juboori et al. (2013) measured from the

peduncopontine tegmental nucleus, the optical parameters used for the BSF curve are explained in the text.

Figure. 5. Experimental results: light transmission in a mouse cortex along the z-axis (a) and the radial axis (b) at 300 μm (blue) and 600 μm (red). The solid lines are the best fit of the BSF model. (c) Surface plot of the simulated light distribution in the slice, obtained with BSF model using the experimentally estimated parameters (μ_s = 211 cm^{-1}, g = 0.86), with overlaid experimental measurements (colors matched to (a) and (b)). Light transmission is in log scale. (d) Contour map of the simulated light distribution.

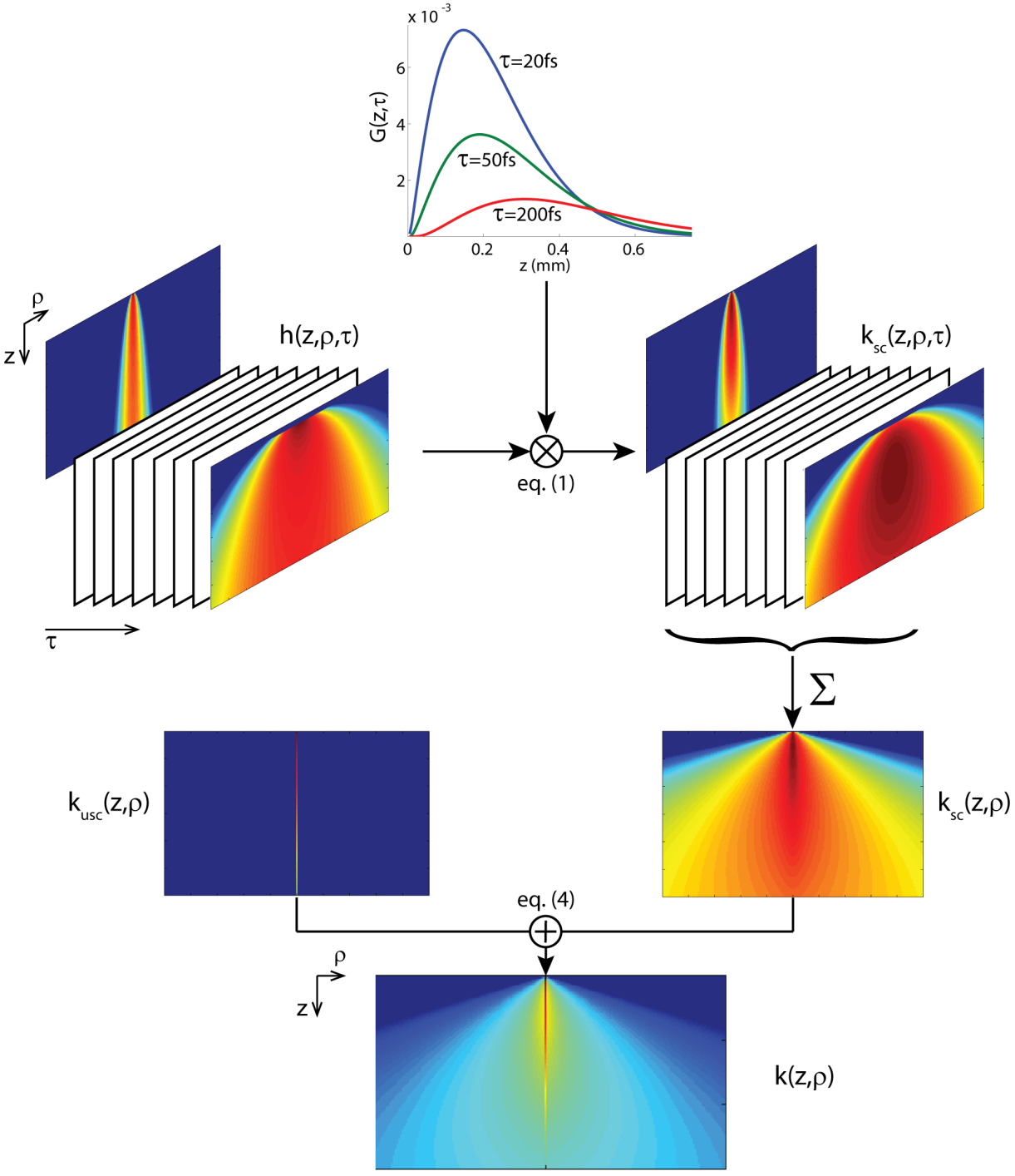

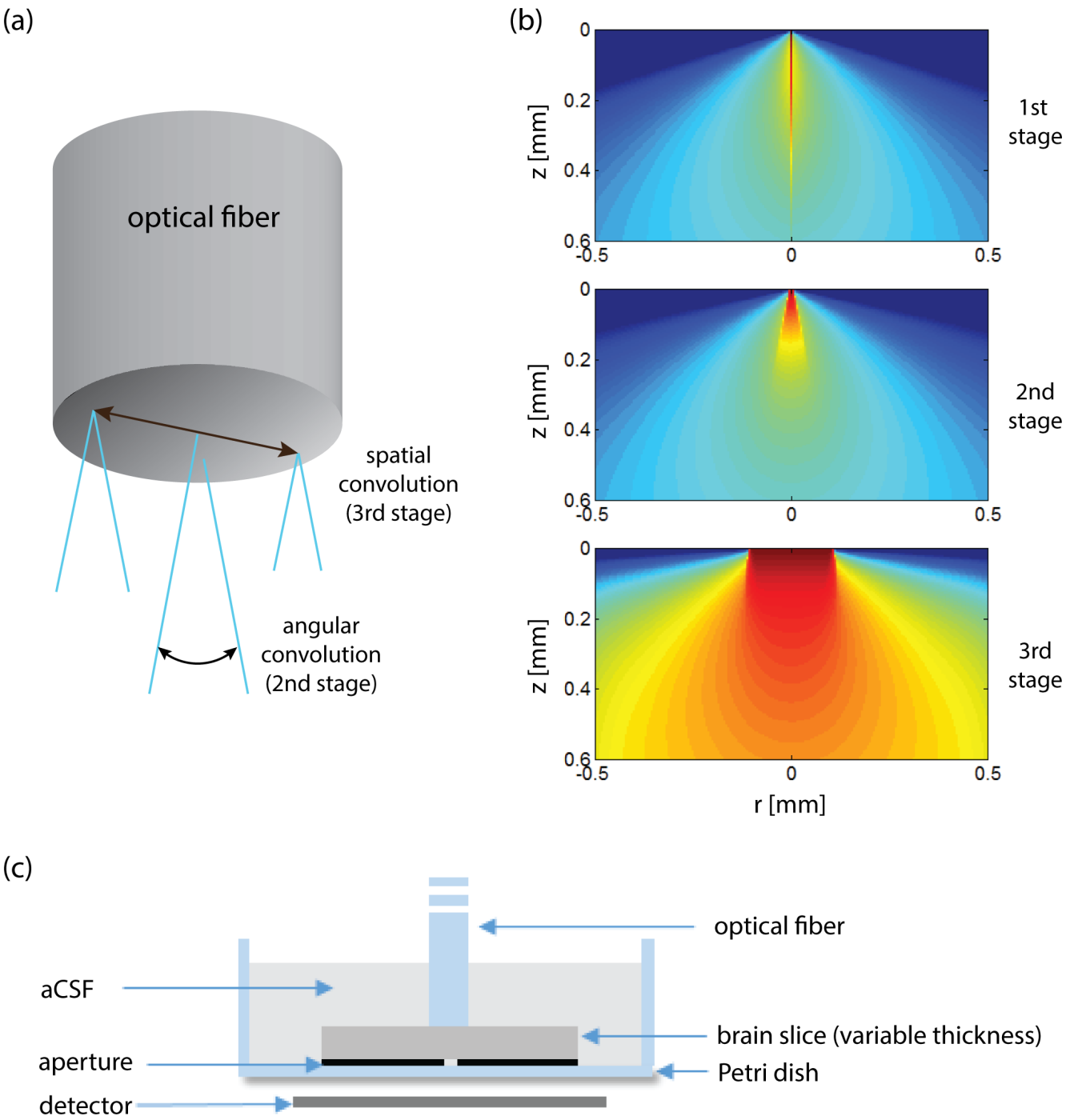

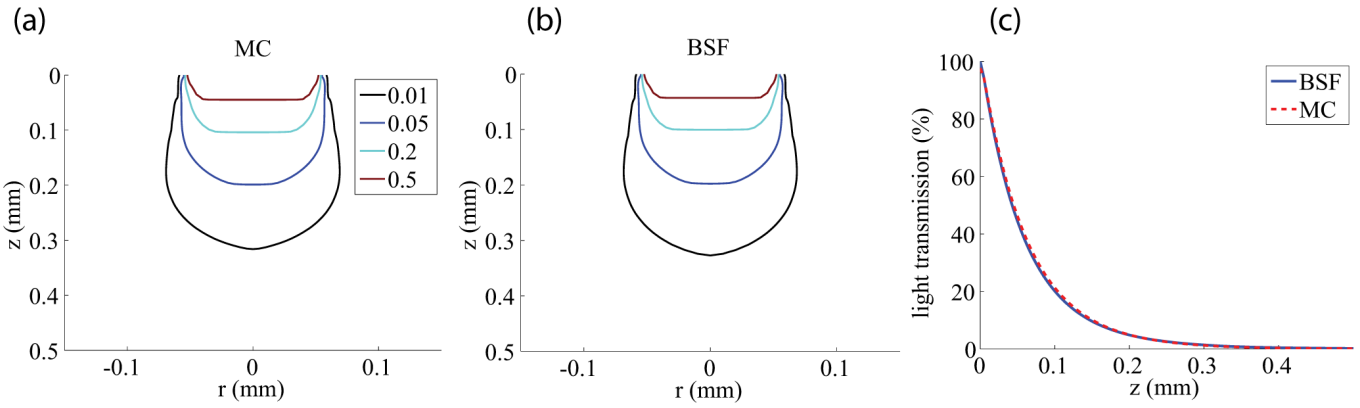

Top panels: scattering coefficient 168.6 cm^{-1}, Al-Juboori et al. (λ = 453 nm)

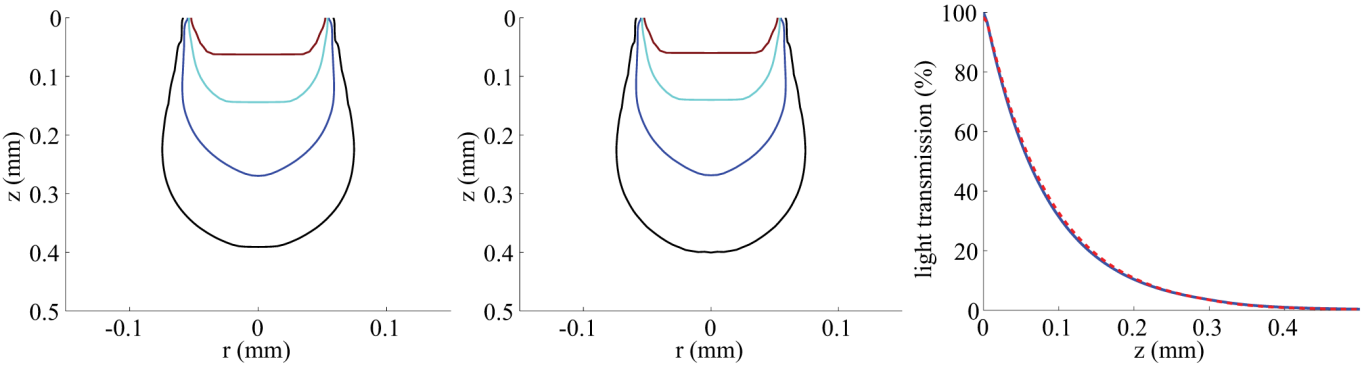

Bottom panels: scattering coefficient 120 cm^{-1}, Yaroslavsky et al. (λ = 480 nm)